

Variation of the low-mass end IMF with velocity dispersion in Early Type Galaxies

using the Porter-14 Semi-Analytical Model

Alexandru-Daniel Taun



university of
 groningen

faculty of science
and engineering



RuG

Kapteyn Institute

Department of Astronomy

Rijksuniversiteit Groningen

Abstract

Variation of the low-mass end IMF with velocity dispersion in Early Type Galaxies using the Porter-14 Semi-Analytical Model

The Initial Mass Function (IMF) is an empirical function that describes the mass distribution of stars formed in a singular star-formation event. This distribution is a probability distribution function (PDF) of the initial masses of stars, in other words, it relates the ratio of low-mass stars to high-mass stars in a stellar population. The IMF has been considered to be universal until recent studies showed that the low-mass end of the IMF varies with galaxy properties, such as velocity dispersion. We used the updated semi-analytical model Porter-14 with the numerical solution of the characteristic mass as a function of external pressure, given by the model of Krumholz (2011), to test if the models reproduce the observations. The results were positive, especially above $\sigma \approx 200 \text{ km s}^{-1}$, and would imply, and therefore enforcing the observations, that there are more low-mass stars in the early-type galaxies than previously thought.

BACHELOR THESIS, UNIVERSITY OF GRONINGEN

SUPERVISOR: PROF. SCOTT TRAGER

June 2017



Contents

1	Introduction	5
2	The Initial Mass Function	6
2.1	The IMF	6
2.2	The form of the IMF	6
2.3	The Galactic IMF	7
2.3.1	The IMF in the solar neighbourhood	8
2.3.2	Open clusters	8
2.3.3	Starburst clusters	9
2.3.4	Galactic center	9
2.4	The characteristic stellar mass	9
3	IMF variations in ETGs	12
3.1	Early Type Galaxies and Velocity Dispersion	12
3.2	Vast population of low-mass stars in ETGs	14
3.3	Relationship between low-mass IMF and velocity dispersion in ETGs	14
4	The Models	16
4.1	Semi-Analytical Models	16

4.2	Porter-14 SAM	17
4.3	Acquiring the data	17
4.4	Data Analysis	18
5	Results and Conclusion	22
5.1	Results	22
5.2	Conclusion	25
6	Appendix	27
6.1	The Python Code	27
6.2	The PDMF mass bins	38
7	References	39



1. Introduction

The quest for understanding how stars form and what is the origin of mass started more than a century ago, with Eddington and Jeans. Star formation happens in gas clouds when parts of the cloud begin to collapse under their own gravity. Due to the collapse, the core of the protostar becomes hotter and hotter until it reaches the temperature that allows hydrogen to burn into helium. This hydrogen burning creates a radiation pressure, which is caused by photons, created in the reaction, being diffused from the core to the outer layers, that counteracts the gravitational collapse and holds the star in balance. Moreover, stars have a spectra of masses, ranging from $0.1M_{\odot}$ to more than $100M_{\odot}$, but is it actually clear what properties of the gas cloud or the environment determine the initial mass of each star? We refer to the initial mass simply because stars loose mass during their lifetime due to a multitude of processes, which are not relevant in this case.

Salpeter E. theoretized that the initial mass of the stars formed in a star-formation event is given by a probabilistic distribution (the initial mass function) and later, this distribution was thought to be universal. However, recent studies (see **Section 3**) showed that this is not case, and the initial mass function is varying with the environment. Krumholz (2011) showed that the external pressure from the interstellar medium onto the gas cloud affects the characteristic stellar mass and it will be later shown that there are more low-mass stars in massive galaxy than previously thought. This would mean that the amount of dark matter in those galaxies is lower than expected and would have great implications in the models of galaxy formation. The question is, can we quantify this variation based on the properties of the galaxy, such as mass or luminosity, and do the updated models reproduce the observed values?

2. The Initial Mass Function

2.1 The IMF

The Initial Mass Function (IMF) is an empirical function that describes the mass distribution of stars formed in a singular star-formation event. This distribution is a probability distribution function (PDF) of the initial masses of stars, in other words, it relates the ratio of low-mass stars to high-mass stars in a stellar population. Therefore, the IMF is a very important tool in studying large populations of stars, such as galaxies, since properties like color, luminosity and lifetime are governed by the initial mass of the star. For example, the high-mass stars are responsible for most the chemical enrichment and the total light of the galaxy, while low-mass stars dominate the total baryonic mass of the galaxy.

The IMF is a key ingredient in Stellar Population Synthesis models (SSP) used to analyze the integrated light of distant galaxies. Since these galaxies are too far away from us to be able to resolve individual stars, the models create an artificial stellar population, with the IMF given as input, in order to recreate the total integrated light from those galaxies. This will provide us with information about the star formation history and the overall evolution of the galaxy. However, it will be shown later that the IMF is not a universal function, but it varies with the star formation environment and other factors. Therefore, a good understanding of these variations is crucial for inferring the physical driving factors, since at the moment, the IMF is an observationally derived relation and the theoretical framework still remains an open question.

2.2 The form of the IMF

In 1955, Edwin Salpeter introduced the notion of IMF, which is described by a power-law form

$$\Phi(\log m) = dN/d\log m \propto m^{-\Gamma} \quad (2.1)$$

where m is the mass of a star and N is the number of stars in some logarithmic mass range $[\log m, \log m + d \log m]$. The normalization constant is derived by setting the integral of the function over a given mass range (usually between $0.1M_{\odot}$ and $100M_{\odot}$) equal to 1. Therefore, if Γ is known, we can calculate the number of stars within a mass interval. Salpeter calculated Γ for the stars in the solar neighbourhood with masses higher than the solar mass and found a value of $\Gamma = 1.35$ (Salpeter 1955). This value is known as Salpeter slope and will be used throughout the paper. What he showed was that the number of stars decreases rapidly with increasing mass. Another way of representing the IMF is in the form of a mass spectrum, in linear mass units

$$\chi(m) = dN/dm \propto m^{-\alpha} \quad (2.2)$$

where it relates to the previous one as

$$\chi(m) = 1/(m \ln 10) \Phi(\log m) \quad (2.3)$$

The relationship between the coefficients is

$$\alpha = \Gamma + 1 \quad (2.4)$$

Later on, it was argued that the IMF was not a single power law over all stellar masses. In 1993, Kroupa et al. found a multisegment power law where the slope of the IMF at lower masses is flatter than the Salpeter value. This segmented IMF will be referred as Kroupa IMF (Kroupa et al 1993). Another way to describe the IMF is by a log-normal distribution in the low-mass end with a power-law tail above $1 M_{\odot}$ (Chabrier 2003). This is known as a Chabrier IMF. These are the main three functional forms proposed to fit the Galactic observations on stellar mass distribution and can be seen in **Figure 2.1**.

Offner et al. (2014) saw the difference in representation as a difference in the underlying physical mechanisms that drive the star formation, whether is a continuous process over all masses (Chabrier) or physical processes of star formation that act differently in separate mass regimes (Kroupa). Another important aspect of the IMF is the high-mass regime where the slope appears to be identical for all star-forming regions in the Local Universe. In this thesis, the focus is on the low-mass regime, where the IMF appears to vary with the conditions of the star-forming region. In this thesis we discuss briefly the Galactic IMF and present and quantify the low-mass end variation of the IMF in ETGs, followed by the comparison with the Porter-14 SAM.

2.3 The Galactic IMF

In this section, we briefly discuss different measurements of the IMF in different stellar population within the disk of the Milky Way galaxy. This includes: volume-limited samples of stars from the vicinity of the Sun, open clusters, starburst clusters and the galactic center. The results are summarized in **Figure 2.2**.

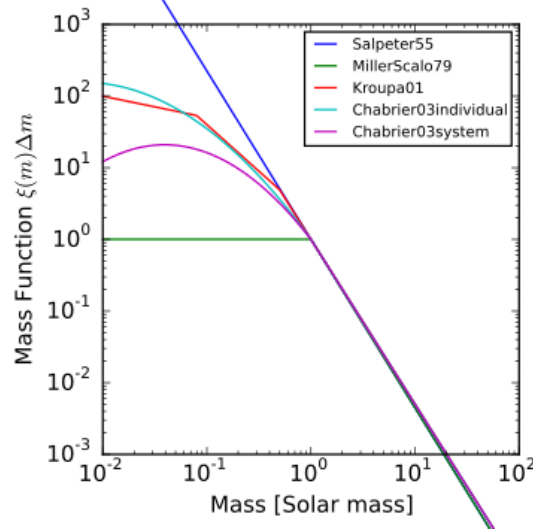


Figure 2.1: The functional forms of the IMF, Salpeter in blue, Kroupa in red and Chabrier in purple (Buchner 2015).

2.3.1 The IMF in the solar neighbourhood

In the late 90's, most of the surveys were limited to a sphere around the Sun with a radius of 5.2 pc. This value was adopted initially by van de Kamp (1971) in his volume-limited surveys. These volume-limited surveys together with a magnitude-limited sample of distant stars allowed Kroupa, Tout and Gilmore in 1993 to establish the basis for the broken power-law fit of the IMF, which later became the Kroupa-type IMF. In 1997, Reid and Gizis used a dataset assembled by Gliese and Jahreiss (1991) to extend the volume-limited sample to a radius of 8 pc. In this sample, the IMF was fit by a power-law with a value of $\Gamma = 0.2 \pm 0.3$ in range $0.1 - 0.7 M_{\odot}$. In the past years, there has been a lot of effort invested to extend the volume-limited sample up to 10 pc. It is expected that the sample will soon be complete and will greatly reduce the uncertainties in the Solar Neighbourhood IMF.

2.3.2 Open clusters

Most of the supersolar ($M_{\star} > 1 M_{\odot}$) IMF studies (e.g., Bonatto & Bica 2007, Maciejewski & Niedzielski 2007, Carraro et al. 2005; Santos, Bonatto & Bica 2005) in these open cluster reported a Salpeter value, however, there are few cases where the reported value was different. These studies were identified by Scalo (2005) and summarized below. In Phelps & Janes (1993), most of the clusters were Salpeter-like with the exception of two, NGC 581 and NGC 663. In 1999, Sanner et al. confirmed a value of $\Gamma = 1.8 \pm 0.2$ for NGC 581, steeper than the Salpeter value, whereas NGC 663 has been studied more recently by Pandey et al. 2005 and Sanner & Geffert 2001 and they found a value of $\Gamma = 2.01 \pm 0.4$. However, they argued that the distance to the cluster, the colors of some of the objects and the dispersion in proper motions were problematic for NGC 663. Other clusters with non-Salpeter slopes are NGC 2422 with a value of $\Gamma = 2.07 \pm 0.08$ (Prisinzano et al. 2003) and NGC 2322 with $\Gamma = 1.94$ (Kalirai et al. 2003). However, both clusters need more

observations in order to confirm their non-Salpeter like nature.

2.3.3 Starburst clusters

Most of these clusters are located at distances of around 3 to 8 kpc, making observations less sensible to details. However, they are crucial tools to determine the IMF variations with environment. The most notable example is the Arches cluster, located at 25 pc away from the Galactic Center, is one of the densest and most massive clusters in our galaxy ($\rho \approx 2 \times 10^5 M_\odot \text{pc}^{-3}$) and has been subjected to many studies. In 1999, Figer et al. measured the IMF above $6M_\odot$ and found a slope flatter than Salpeter ($\Gamma = 0.65$). Using different techniques, Stolte et al. (2002) found a slightly steeper slope ($\Gamma = 0.8$), but still flatter than Salpeter. The most recent result comes from Espinoza, Selman & Melnick (2009), who after paying close attention to differential extinctions, they reported a value of $\Gamma = 1.1 \pm 0.2$.

Other clusters have been studied as well, such as Westerlund 1. Westerlund 1 is the most massive known young cluster (4-7 Myr) in the galaxy. Brandner et al. (2008) analyzed this cluster and found $\Gamma = 1.3$ in the mass range $3.4\text{--}27M_\odot$ for the inner parts, which is consistent with the Salpeter value. Many other starburst clusters have been studied and strong evidence was found to support a radially varying mass function, which is explained by the mass segregation.

2.3.4 Galactic center

Most (or maybe all) galaxies inherit a massive black hole at the center of the galaxy. Our central black hole has a mass of $\approx 3 \times 10^6 M_\odot$ (Ghez et al. 2003, Schodel et al. 2003) which stops the cold molecular clouds from collapsing due to its massive tidal forces (Morris 1993). Therefore, the shape of the IMF is very different from other places in the galaxy. There have been many studies conducted to observe the IMF at the GC (Galactic center) but the results are inconclusive due to the high opacity of the clouds surrounding the GC. Most of these studies reported an extremely flat (top-heavy) IMF which suggest a large production of stellar mass black holes. However, the presence of these stars is inconsistent with stellar motion observations (Loeckmann, Baumgardt & Kroupa 2010). Further observations are needed to understand this behavior, especially in the low-mass and, to be able to explain the low-mass stars deficit.

2.4 The characteristic stellar mass

It is believed that the characteristic mass of stars can be computed in terms of only fundamental constants, since it depends on the characteristic fragment mass in a star forming cloud which is set by the cloud's density and temperature profile. This view was supported by observations that suggested a small or non-existent variation of the characteristic mass with the star-forming environment. Krumholz (2011) computed the characteristic stellar mass almost entirely in terms of fundamental constants with what he considered to be a

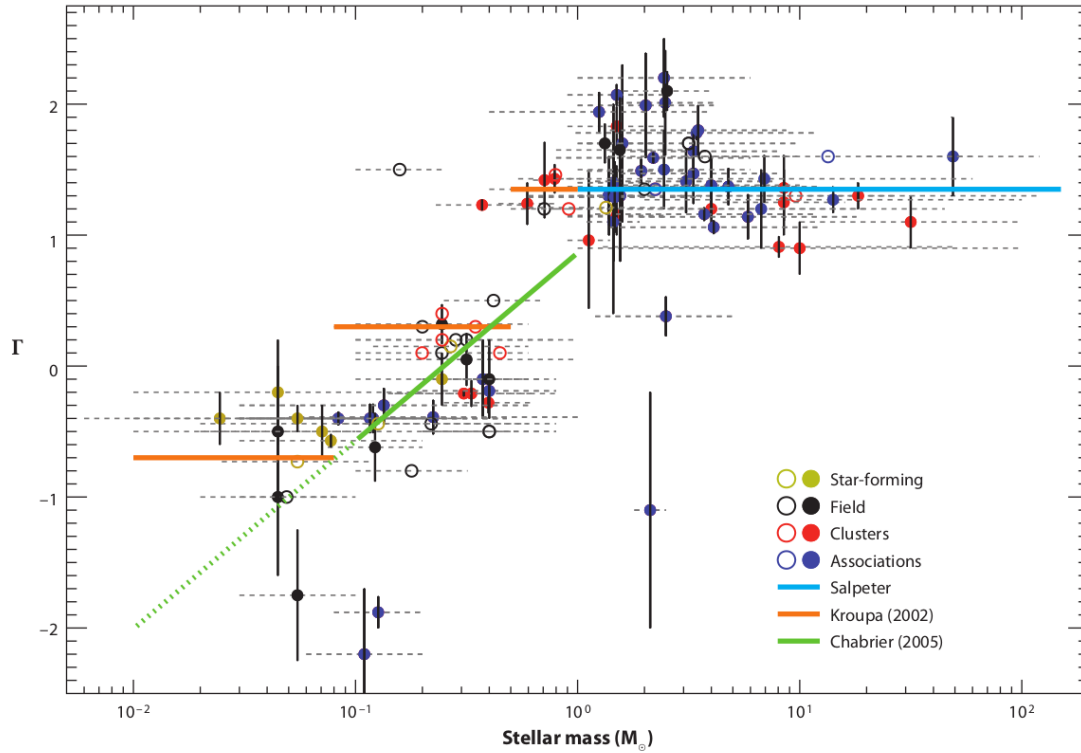


Figure 2.2: This plot shows the derived IMF slope Γ from different stellar populations.

The points are located at the center of the mass bin used to derive the slope. The data points are from multiple studies on the Galactic IMF. These papers are discussed in more detail in Bastian et al. 2010. Image credit: Bastian et al. 2010

weak dependence on the interstellar pressure. For the calculation, he assumed a region of a gas cloud with a pressure P that starts to collapse under its own gravity. Since the dynamical timescale varies as $t_{dyn} \approx \frac{1}{\sqrt{G\rho}}$, the central part of the protostar will collapse faster due to its higher density. Therefore, the surrounding gas will either accrete or collapse separately, depending on the pressure. The pressure near the star will be higher due to the radiation heating, making the gas resistant to fragmentation and force it to accrete onto the protostar. Far away from the star, the pressure will be lower and the gas colder, therefore is more likely that it will collapse independently to form other stars. Thus, the limit where the gas will accrete rather than fragment is considered to be the characteristic stellar mass. Based on the deuterium burning physics and approximations of stellar equations, such as polytropic models, he calculated the characteristic stellar mass as a function of interstellar pressure P (see **Figure 2.3** - red dotted line):

$$M_* = 0.15 \left(\frac{P/k_B}{10^6 \text{K cm}^{-1}} \right)^{-1/18} M_\odot \quad (2.5)$$

Initially, it seems to be counterintuitive but if the external pressure increases, the gas will not accrete but rather fragment to form other stars. In other words, the higher the external pressure is, the lower the characteristic mass will be and more low-mass stars will form. In the analytical description of the process, the dependence with external pressure is very small. However, when using a numerical instead of a polytrope model for stellar profile (**Figure 2.3**: blue solid line), the characteristic stellar mass varies, on average, with ≈ 1.5 orders of magnitude. What seems to be a small variation, will be later shown that greatly influences the low-mass end of the IMF.

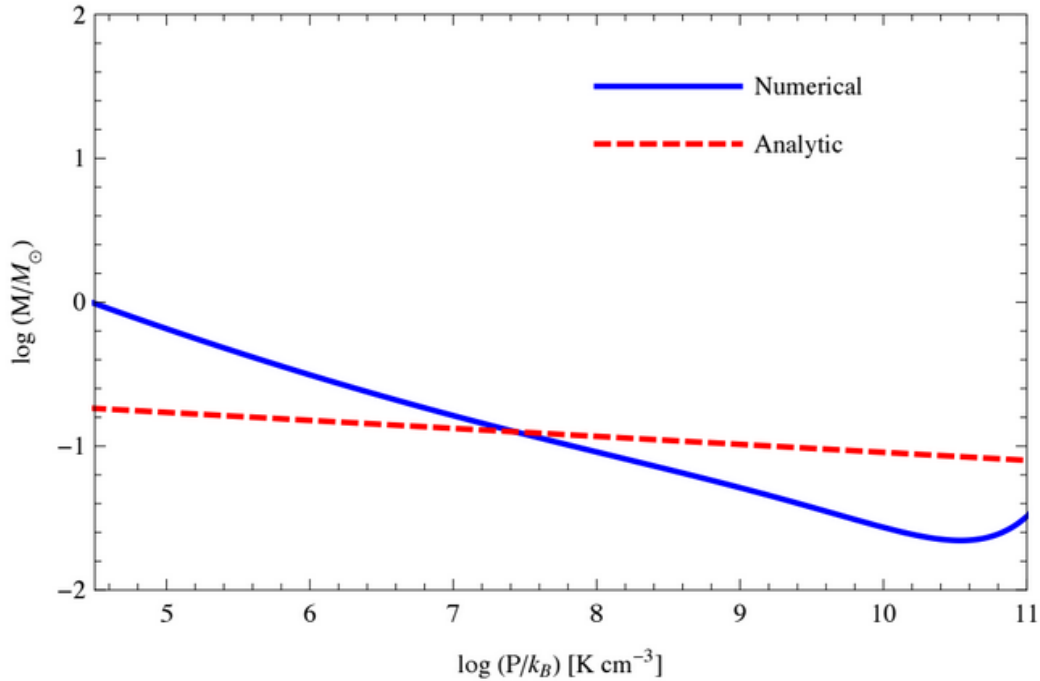


Figure 2.3: Characteristic stellar mass M as a function of interstellar pressure P . A comparison of the numerical and analytical solution. Image credit: Krumholz (2011)



3. IMF variations in ETGs

3.1 Early Type Galaxies and Velocity Dispersion

Early Type Galaxies (or ETGs) are a class of galaxies that include the elliptical and S0 type galaxies. Elliptical galaxies are one of the three main categories of galaxies described by Hubble (Hubble 1936). They have an ellipsoidal shape and an almost featureless and smooth brightness profile (see **Figure 3.1**). Compared to spiral galaxies, most of the elliptical galaxies are much older and more massive. They are mostly composed of old, low-mass stars with a hot interstellar medium and minimal or non-existent star formation activity.

S0 galaxies, or lenticular galaxies, are morphologically between elliptical and spiral galaxies. The similarity with spiral galaxies comes from the presence of the bulge and the disk, however, they do not exhibit spiral arms or considerable amounts of interstellar medium, which is a characteristic of elliptical galaxies. Therefore, the elliptical and S0 galaxies (the ETGs) are perfect candidates for measuring the IMF due to their low or non-existent star formation activity.

In astronomy, the velocity dispersion - σ - is a statistical quantity which describes the spread of velocities around the mean values for different types of objects such as clusters or galaxies. It is a very important tool in calculating the mass of a gravitational bound object, from the virial theorem, or the luminosity of an elliptical galaxy, using the Faber-Jackson relation (Faber & Jackson 1976).

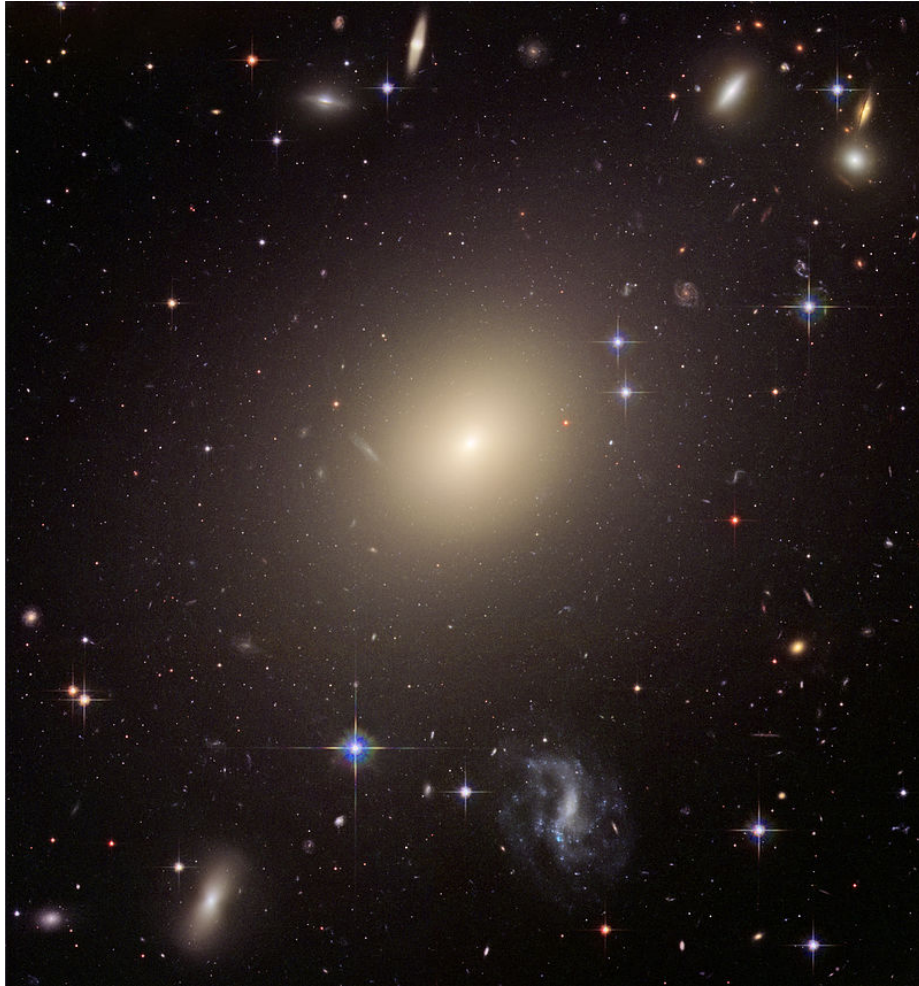


Figure 3.1: The giant elliptical galaxy ESO 325-G004 (NASA, ESA, and The Hubble Heritage Team)

The small luminosity of low mass stars makes the direct observation of them impossible in the extragalactic environment, therefore the low-mass end of the IMF was assumed to be the same everywhere in the Universe. However, recent studies on the extragalactic IMF have shown that this is not the case. The low-mass IMF of Early-Type Galaxies varies, therefore becomes more dwarf-rich with increasing galaxy velocity dispersion (Auger et al. 2010; Conroy and van Dokkum 2012a,b; Ferreras et al. 2013; LaBarbera et al. 2013; Spiniello et al. 2014, 2012; Treu et al. 2010; van Dokkum and Conroy 2010). The first modern observation of the low-mass IMF variation was done by Pieter van Dokkum and Charlie Conroy, 2010.

3.2 Vast population of low-mass stars in ETGs

van Dokkum & Conroy (2010) used surface gravity sensitive spectral line strengths indicative of low mass stars ($\leq 0.3M_{\odot}$), more specifically the Na doublet ($\lambda = 0.8183 \mu m$ and $\lambda = 0.8195 \mu m$, Faber and French 1980, Schiavon et al. 1997) and the Wing-Ford molecular FeH band ($\lambda = 0.9916 \mu m$ Wing and Ford 1969, Schiavon et al. 1997), and compared them with the ones created with the SSP models to get the best IMF fit. Their result can be seen in **Figure 3.1** and it is clear that a Kroupa IMF, which fits our galactic IMF, does not give a large number of low-mass stars in order to reproduce the line strengths. A more bottom-heavy IMF is needed and they found a value for the slope of 3 (or $\Gamma = 2$) which is much steeper than Salpeter coefficient of 2.35 but fits the data extremely well.

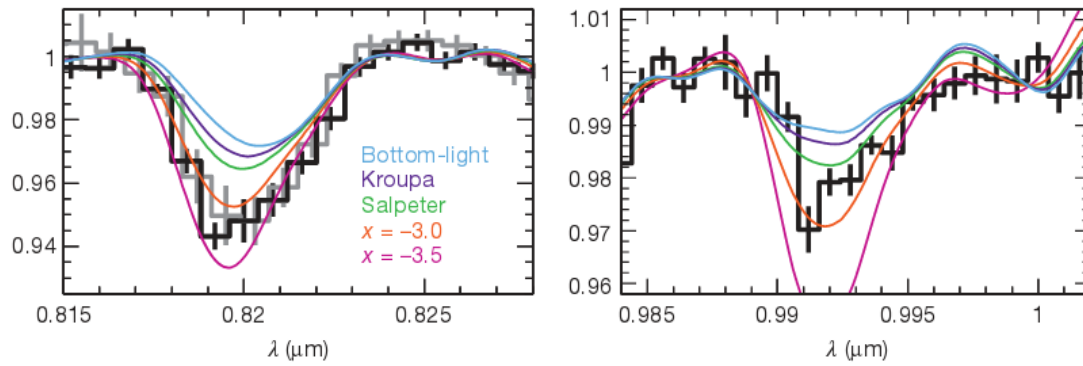


Figure 3.2: IMF fits for the Na I (left) and Wing-Ford (right) spectral regions. Image credit: van Dokkum and Conroy (2010)

Spiniello et al. (2012) found that the Na doublet lines can be influenced by interstellar absorption which implied that the number of low-mass stars in ETGs was not as large as previously thought. However, later on, using a similar relation, this time involving the TiO2 line strengths which are sensitive to cool dwarf stars and less influenced by the metallicity, the same trend of a bottom-heavy IMF was found (Spiniello et al. 2014).

3.3 Relationship between low-mass IMF and velocity dispersion in ETGs

The spectral lines used in previous studies (such as NaI, Wing-Ford FeH, CaI, etc.) are mostly in the red-optical and Near-Infrared (NIR) parts of the spectrum. The NIR spectra is contaminated by the presence of the sky lines and telluric absorption from water vapour and the equivalent width in the red spectra relies heavily on correct removal of these line, therefore making the analysis of the SSP models more difficult. Since optical spectra are easier to obtain with current spectrographs, the blue-optical spectras are the perfect choice due to their less uncertainties in the models.

Spiniello et al.(2014) used 7 features, the bTiO, aTiO, NaD, TiO1, TiO2, CaH1 and CaH2. These are present in the spectrum, ranging from 350 to 750nm. In this wavelength

range, the change in the number of dwarf stars in the galaxy is influenced and similar to the change in the effective temperature of the cool red giant (RGB) population. Moreover, spectra of galaxies from the SDSS galaxies were stacked for different velocity dispersion (in bins of 150, 190, 230, 270, 310 km/s with ± 20 km/s) and were compared to with CvD12 SSP models with same age (13.5 Gyr) and solar metallicity but with different IMF slopes.

From the stacked spectra, the equivalent widths were measured for each indicator in each σ bins and it was found that all indicators showed a steeper IMF slope with increasing galaxy mass. This means that the IMF in least-massive galaxies ($\sigma_* \propto 150$ km/s) is fitted by a Chabrier IMF, in the intermediate mass galaxies ($\sigma_* \propto 230$ km/s) by a Salpeter IMF and by a bottom-heavy IMF for the most massive galaxies ($\sigma_* \propto 310$ km/s). The best-fitting IMF slope for each σ bin is showed in Figure 3. By using a linear regression model of the form:

$$x = a \times \log \sigma_{200} + b \quad (3.1)$$

the relation between the IMF slope (x) and the central stellar velocity dispersion (σ) was determined:

$$x = (2.3 \pm 0.1) \log \sigma_{200} + (2.13 \pm 0.15) \quad (3.2)$$

These values will be compared to the ones from the Porter-14 SAM in the Results section.

A visualization of the cosmic web, showing a complex network of dark matter filaments and galaxy clusters. The filaments are colored in shades of blue, green, and yellow, while the clusters are bright orange and red. A central bright blue and white point represents a high-density region.

4. The Models

4.1 Semi-Analytical Models

Treating the process of galaxy formation in full detail on a computer has always been a challenge for astronomers. The problem comes from the nonlinear aspects of the physics involved, for example: implementing Newton's equations in an expanding Universe together with non-gravitational effects such as heating and cooling by radiation. All these processes are computationally expensive. One solution lies in "semi analytic modeling" or "phenomenological galaxy formation modeling" (Benson 2010), which treats the various physical processes associated with galaxy formation using approximate, analytic techniques. The complexity of the physics being treated influences the degree of approximation in the N-body simulations. The precision can vary from well-calibrated estimates of dark matter merger rates to large parameter uncertainties in scaling functions (Benson 2010).

Compared to N-body simulations, the semi-analytic approach is computationally cheap. However, the biggest disadvantage is that the semi-analytic modeling incorporates a larger degree of approximation, yet comparison studies of semi-analytical vs. N-body simulation have shown good agreement with the exception of simplified physics (Benson et al 2001b; Yoshida et al. 2002; Helly et al. 2003b) and simulations of individual galaxies (Stringer et al. 2010). Semi-analytic models have been used to investigate many aspects of galaxy formation including: galaxy counts (Kauffmann et al. 1994; Devriendt and Guiderdoni 2000); abundance and properties of Local Group galaxies (Benson et al. 2002b; Somerville 2002; Li et al. 2010) and the reionization of the Universe (Devriendt et al. 1998; Benson et al. 2001a; Somerville and Livio 2003; Benson et al. 2006).

4.2 Porter-14 SAM

The first theoretical framework of the semi-analytical modeling originated in the work of White and Rees (1978). The first version of the semi-analytical model of galaxy formation used in this work was presented in Somerville & Primack (1999) and Somerville, Primack & Faber (2001). Since then, due to scientific discoveries, noteworthy updates followed, such as Somerville et al. (2008b, S08), Somerville et al. (2010), Popping, Somerville & Trager (2014, PST14), Porter et al. (2014), and Somerville, Popping & Trager (2015, SPT15). The model follows the clustering of dark matter halos and other important physical processes such as shock heating and radiative cooling of gas, supernovae feedback, star formation, active galactic nuclei (AGN) feedback (by quasars and radio jets), metal enrichment of the interstellar and intracluster medium, mergers of galaxies and the evolution of stellar populations (Popping et al. 2016).

The time evolution of each of these baryonic components is governed by a set of differential equations, which also tracks the mass of the components. In other words, the SAMs follow the flows of matter between different components. In models presented above, the galaxies form within a dark matter halo and include "hot" gas which is assumed to be in a quasi-hydrostatic spherical configuration around the virial radius of the halo, "cold" gas in a thin disk and "ejected" gas which has been heated and ejected from the halo by stellar winds. Galaxies that form at the center of halos are called "central" galaxies. When the dark matter halos merge, the central galaxies of small halos become "satellite" galaxies and orbit the larger halo until they merge with the central galaxy of the larger halo or they are destroyed by the tidal forces. The version of the SAM that I use is a modified version of the Porter-14 SAM (Porter et al. 2014) that includes the numerical solution (instead of the analytical one) of the characteristic stellar mass as a function of interstellar pressure (Krumholz 2011), discussed in **Section 2.4**.

4.3 Acquiring the data

For this project, I ran five simulations with different dark matter halo merger histories. The merger histories are based on numerical simulation, the isotrees (Klypin et al 2011; Trujillo-Gomez et al. 2011) and not on Monte Carlo realizations. Initially, I used only isotrees 0 and 1 since the number of galaxies produced by isotree 0 was much larger, I ran the simulation twice with the isotree 1 to get a balance in the data. Since the galaxies produced with different isotrees are slightly different, it was decided that I should run two more simulations with new isotrees. The simulation number, the isotree used and the total number of galaxies produced are presented in **Table 4.1**

Form the output of each simulation, I have only used the **present day mass function** (*pdmf.dat*) and **properties** (*galprop.dat* for the metallicities) files. After importing the data, the next step was to select galaxies that match those from Spiniello et al. (2014). The first condition used was that galaxies have little or non-existent star formation activity ($SFR/M_{\odot} < 10^{-11} \text{yr}^{-1}$). The second one is concerned with the velocity dispersion σ of the bulge. From these, the galaxies with $130 \leq \sigma \leq 330 \text{ km/s}$ were selected. However,

Number of simulation	Isotree used	Galaxies produced
1	Isotree 0 0 1	≈ 14.300
2	Isotree 0 0 1	≈ 14.300
3	Isotree 0 0 0	≈ 22.300
4	Isotree 0 0 2	≈ 19.800
5	Isotree 0 0 3	≈ 10.000

Table 4.1: Summary of Simulations

due to peculiar properties of galaxies, such as high velocity dispersion in the low-mass regime, galaxies between $8 \leq \log M_* \leq 9$ were removed as well. After all these conditions were applied, we were left with 2900 galaxies for the following analysis. For a better visualization of the simulation output, histograms of galactic mass (M_*) and metallicity (Z_*) were plotted in **Figure 4.2**. It can be clearly seen that the mass and metallicity both increase with increasing velocity dispersion, in good agreement with observations.

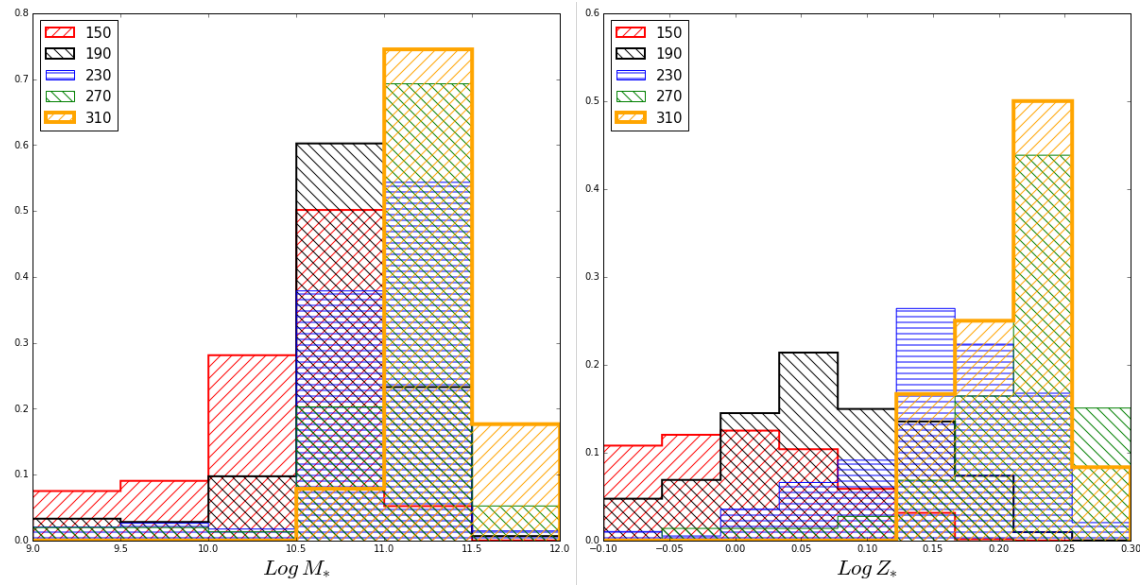


Figure 4.1: Histograms of mass (left) and metallicity (right), both logarithmic, for each σ bin. For the mass histogram, 6 bins were used between 9 and $12 \log M_\odot$ with size 0.5. For the metallicity histogram, 9 bins were used between -0.1 and $0.3 \log Z_\odot$ with size 0.045.

4.4 Data Analysis

The PDMF in the output was given as the fraction of mass in stars in logarithmic mass bins, ranging from 0.1 to $1.8 M_\odot$ ($dM/d\log M$). Since we were interested in the numerical fraction ($dN/d\log M$), the PDMF value in each mass bins was divided by the mean mass in that bin. The mass bins are given in linear space but equally spaced in logarithmic space

and the values can be seen in the Appendix.

$$dN/d\log M = dM/d\log M \times \frac{1}{M_{mean}} \quad (4.1)$$

To understand how the IMF in the simulation compares with the median, 15 galaxies were selected at random for each velocity dispersion bin and their IMF was plotted, with the median IMF plotted on top. This can be seen in **Figure 4.3**.

The next step in the analysis was to calculate the slope of the low-mass end IMF in each σ bin. This was done by separating the galaxies with respect to their velocity dispersion and then calculating the median value in each mass bin, as well as the standard deviation. Since the IMF is described by a power-law, in log-log space the function becomes a line. Therefore, lines of the form $ax + b$ were fitted to the resulting IMF using the least-square method. For the fitting, 3 mass ranges were used: $0.1 - 0.7M_{\odot}$, $0.1 - 0.4M_{\odot}$ and $0.4 - 0.7M_{\odot}$. The median values in each mass bin, including the standard deviation and the line fit for each σ bin as well as a comparison between all 5 IMFs can be seen in **Figure 4.4**. The slope values will be compared in the Results and Conclusion section.

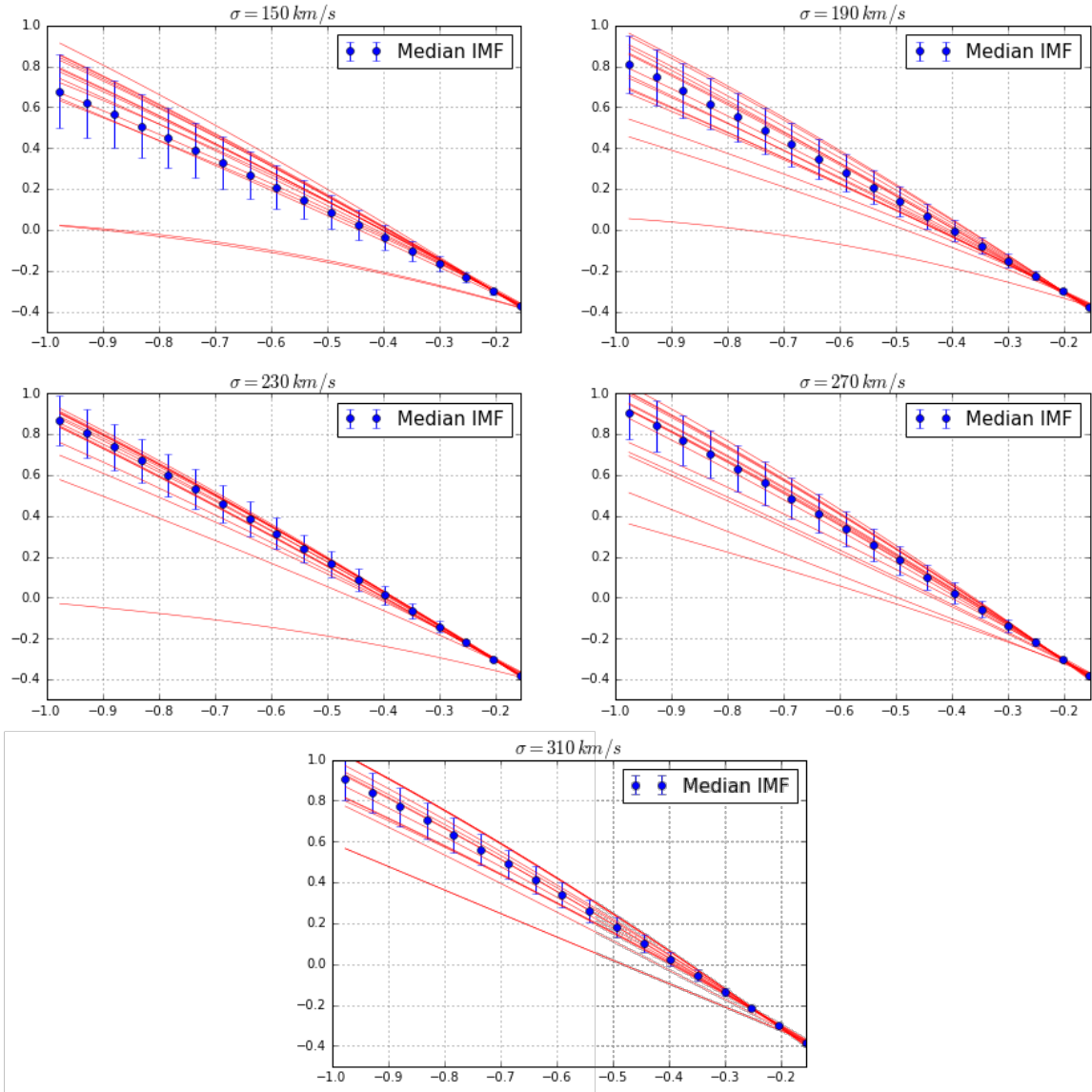


Figure 4.2: The median IMF (blue dots) in each velocity dispersion bin plotted on top of the IMF of 15 random selected galaxies (red lines). The x axis is $\text{Log } M_*$ and y axis is $\text{Log}(\frac{dN}{d\text{Log } M_*})$.

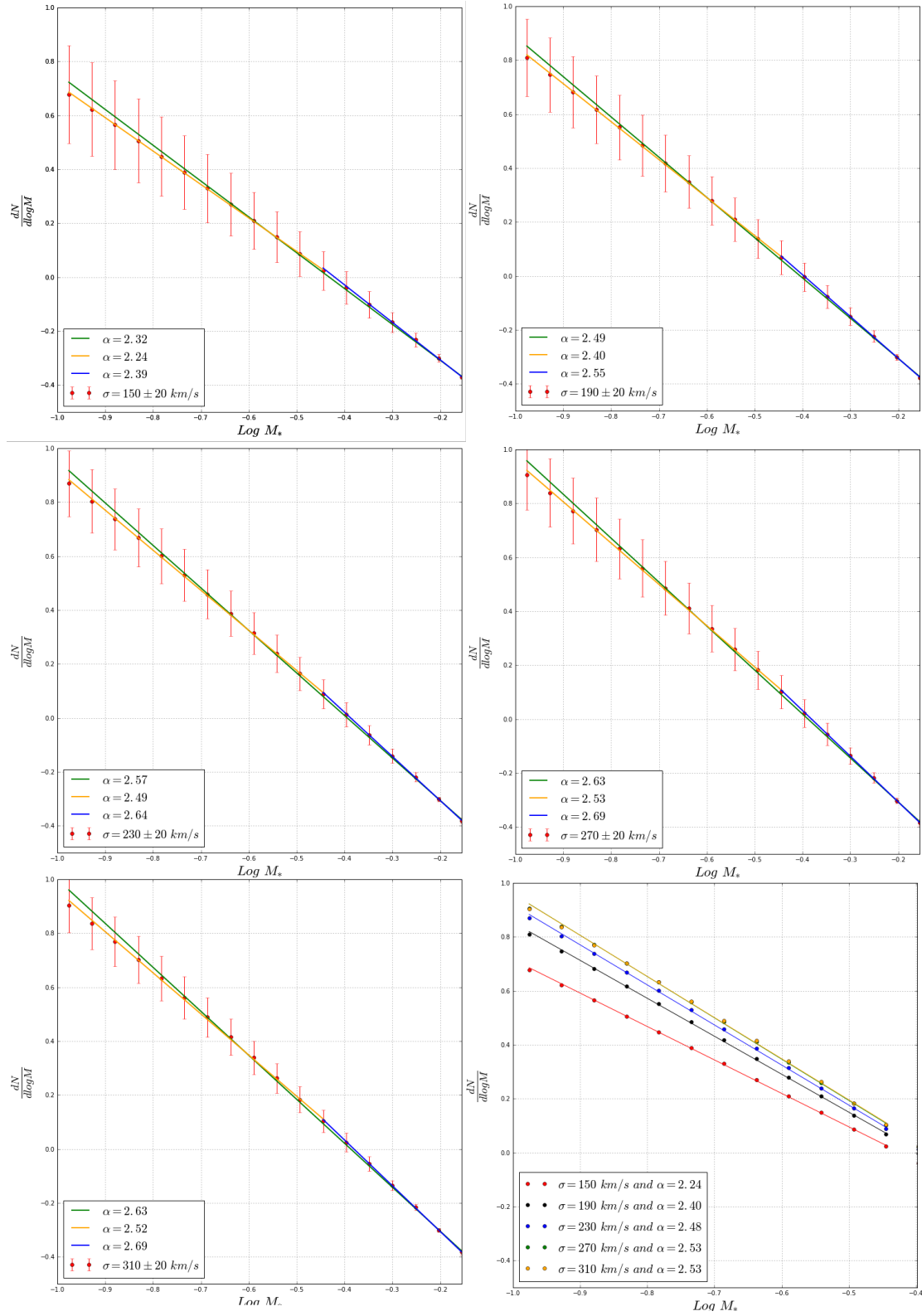


Figure 4.3: Plots of the median IMF (red dots) in each velocity dispersion bin and line fits for 3 mass ranges: green: $0.1 - 0.7 M_\odot$, yellow: $0.1 - 0.4 M_\odot$ and blue: $0.4 - 0.7 M_\odot$. *Bottom Right:* A comparison between all 5 median IMFs in the $0.1 - 0.4 M_\odot$ mass range.

5. Results and Conclusion

5.1 Results

In this section I present the relationship between the the low-mass end IMF slope and the velocity dispersion σ , followed by the comparison with state-of-the-art observations of Spiniello et al. (2014). As can be seen in **Table 5.1**, the slope of the IMF increases with increasing velocity dispersion. This implies that there will be more low-mass stars in more massive galaxies.

Velocity dispersion σ (km/s)	0.1-0.7 M_{\odot}	0.1-0.4 M_{\odot}	0.4-0.7 M_{\odot}
150	$\alpha=2.33$	$\alpha=2.24$	$\alpha=2.39$
190	$\alpha=2.49$	$\alpha=2.41$	$\alpha=2.55$
230	$\alpha=2.57$	$\alpha=2.48$	$\alpha=2.63$
270	$\alpha=2.63$	$\alpha=2.53$	$\alpha=2.69$
310	$\alpha=2.63$	$\alpha=2.52$	$\alpha=2.70$

Table 5.1: The low-mass end IMF slopes from the fit done in section 4.

The values from **Table 5.1** are plotted in **Figure 5.1**, together with the data from Spiniello et al. (2014). It can be seen that above $\sigma = 200 \text{ km/s}$, models fit the observed values very well, within one standard deviation. Below this value, the models are more Salpeter-like, whereas the observed are closer to a Chabrier IMF. This would imply that the models are more dwarf-rich and one explanation would be that the galaxies with small velocity dispersion selected from the simulations are not similar to the ones from Spiniello et al. (2014). To check if this is the case, a more detailed analysis of the data would be required. However, the aim of this work was to check if the difference of ≈ 1.5 orders of magnitude between the numerical and analytical solution (see **Section 2.4**) is actually significant, since the stellar mass range spans ≈ 3 orders of magnitude (from $\approx 0.1 M_{\odot}$ to

$\approx 100M_{\odot}$) and a deviation of 1.5 orders is substantial.

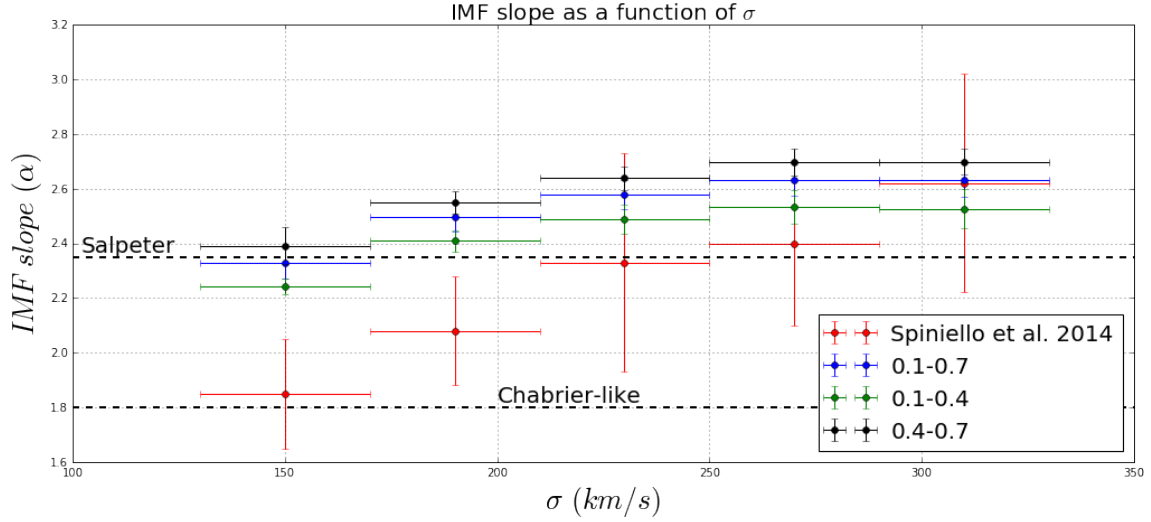


Figure 5.1: Comparison between the IMF slopes of Spiniello et al. (2014) (*red dots*) and this work: *green dots*: between $0.1 - 0.4M_{\odot}$, *black dots*: between $0.4 - 0.7M_{\odot}$ and *blue dots*: between $0.1 - 0.7M_{\odot}$. The error bars of this work are given as 5σ uncertainty due to very small values.

In **Figure 5.2** I present the values for the analytic solution. These were calculated by Gergo Popping. As it can be seen, the result of the analytic solution is extremely flat and the ratio of low mass stars created does not vary with galactic mass. Even if this would be the case, the small variation implies that a measurement will be almost impossible due to the high uncertainties (as seen in Spiniello et al. 2014). In **Figure 5.3** I present the comparison between the IMF slopes calculated using numerical and analytical solution. The difference is not substantial, however the numerical solution trend is much steeper and it could actually be measured. This variation allowed us to reproduce the relation between the IMF slope and the velocity dispersion reasonably well and to support the fact that the external pressure on a star-forming cloud has greater implications than previously thought. If this true, then the number of low-mass stars in early type galaxies is higher and would imply that the amount of dark matter is lower, therefore the models of galaxy formation have to be changed in order to account for this.

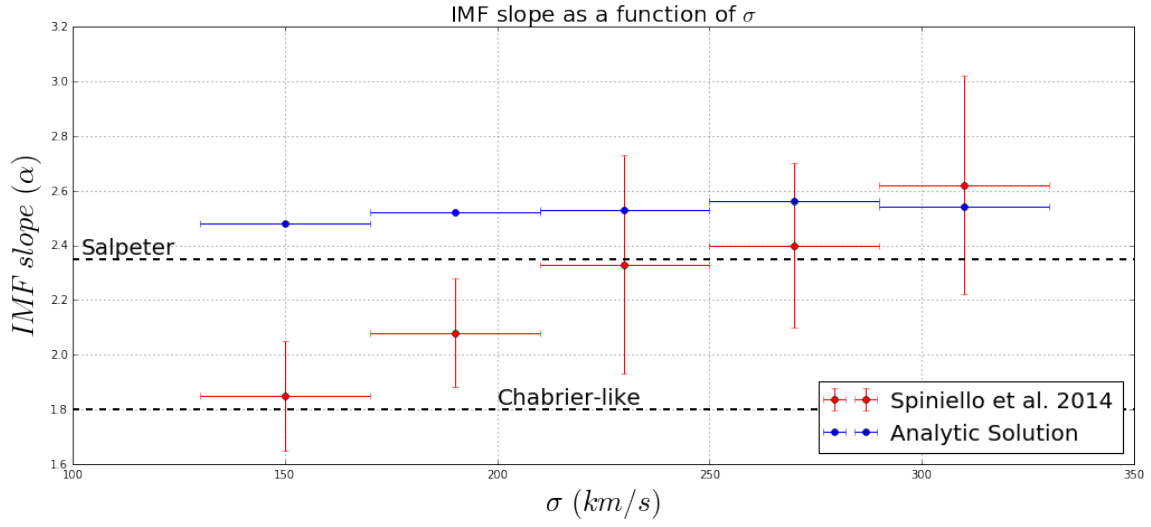


Figure 5.2: Comparison between the IMF slopes of Spiniello et al. (2014) (*red dots*) and the IMF slopes derived using the analytic solution.

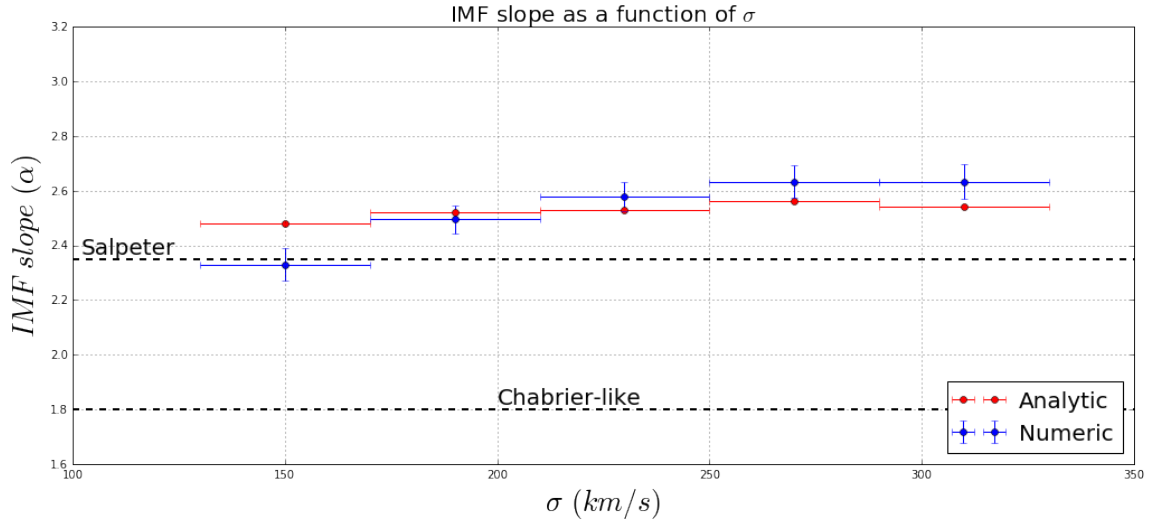


Figure 5.3: Comparison between the IMF slopes derived using the numerical solution (this work, in *blue*) and the analytic solution (*red*). The slopes were calculated in approximately the same range of $0.1M_{\odot}$ to $\approx 0.7 - 1M_{\odot}$.

5.2 Conclusion

The Initial Mass Function is an empirical function that describes the mass distribution of stars after a single star-formation event. In other words, it relates the ratio of high-mass stars to low-mass stars. The IMF is a crucial tool in understanding the evolution of large population of stars, such as galaxies, since high-mass stars are responsible for most of the light of the galaxy, whereas low-mass stars highly contribute to the total baryonic mass of the galaxy. Due to observational limitations, in the beginning, the IMF has been studied only in the Milky Way galaxy. From these observations, the IMF has been described by a power-law in the high-mass end with a log-normal turn over and an exponential cut-off below $1 M_{\odot}$. The IMF has been considered to be universal until recent studies showed that the low-mass end of the IMF varies with galactic properties, such as velocity dispersion. More precisely, the studies revealed that early-type Galaxies with high velocity dispersion have more low-mass stars than previously predicted by the universal IMF. Overall, the IMF is an observational derived relation and the actual physical framework is still unclear. Recent theories on low-mass fragmentation due to turbulence (Krumholz 2011) have been implemented in the Porter-14 semi-analytical model. Until now, the analytic solution of the relationship between the characteristic mass and external pressure was used. Recent state-of-the-art measurements showed that the trend is much steeper. Therefore, the numerical solution, which is steeper, was implemented in the models. It seems to recreate the observed to a good extent, especially in the high velocity dispersion region ($\sigma \geq 200$ km/s) and would imply that the number of low-mass stars in early type galaxies is higher than previously thought. Therefore, the amount of dark matter used in the models of galaxy formation will have to change to account for this difference. For future research, a more detailed analysis of the simulations and better selection criteria are required in order to compare the same populations of galaxies. It would give a better insight into how the IMF varies with the galactic properties and it will change the old method of implementing an universal IMF in the models of galaxy formation.

Acknowledgements

I would like to thank my supervisor Scott Trager for his optimism and the ability to explain the subject really well, and I was very glad to hear that he already planned a subject for my thesis, before asking him. It showed that he trusts me and my capabilities, and therefore it boosted my confidence and motivation. I would also like to thank Gergo Popping for helping me understand how to run a simulation and how to use the data. Moreover, I would like to thank all members of Kapteyn Institute, both staff and students, for being part of a great community. Now, going back in time, I want to thank my primary school physics teacher, Prof. Elena Seciu for her devotion to teaching me physics, even after I finished school. I would also like to thank Ovidiu J. Tercu for giving me the chance, before coming to the university, to learn more about the observational astronomy. The last, but not the least, I would like to thank my parents for their amazing commitment in helping me pursuing my dream of studying astronomy.

6. Appendix

6.1 The Python Code

```
1  """
2  Code written by Alexandru-Daniel Taun for the Bachelor thesis year 2017
3  """
4
5  import scipy.stats as ss
6  import pandas as pd
7  import numpy as np
8  from __future__ import print_function, division
9  import matplotlib.pyplot as plt
10 import scipy.optimize as opt
11 %matplotlib inline
12 np.set_printoptions(precision=13)
13
14 #Import the data. Import every simulation as a matrix
15 #Isotree 1
16 data1 = pd.read_csv("pdmf1.dat", sep=' ', comment='#', header = None)
17 data1 = data1.as_matrix()
18 #Isotree 1
19 data2 = pd.read_csv("pdmf2.dat", sep=' ', comment='#', header = None)
20 data2 = data2.as_matrix()
21 #Isotree 0
22 data3 = pd.read_csv("pdmf3.dat", sep=' ', comment='#', header = None)
23 data3 = data3.as_matrix()
24 #Isotree 2
25 data4 = pd.read_csv("pdmf4.dat", sep=' ', comment='#', header = None)
26 data4 = data4.as_matrix()
27 #Isotree 3
28 data5 = pd.read_csv("pdmf5.dat", sep=' ', comment='#', header = None)
29 data5 = data5.as_matrix()
```

```

#Import galprop.dat for each simulation
31 #Isotree 1
   g_prop1 = pd.read_csv("galprop1.dat", sep=' ',comment='#', header = None
   )
33 g_prop1 = g_prop1.as_matrix()
   #Isotree 1
35 g_prop2 = pd.read_csv("galprop2.dat", sep=' ',comment='#', header = None
   )
   g_prop2 = g_prop2.as_matrix()
37 #Isotree 0
   g_prop3 = pd.read_csv("galprop3.dat", sep=' ',comment='#', header = None
   )
39 g_prop3 = g_prop3.as_matrix()
   #Isotree 2
41 g_prop4 = pd.read_csv("galprop4.dat", sep=' ',comment='#', header = None
   )
   g_prop4 = g_prop4.as_matrix()
43 #Isotree 3
   g_prop5 = pd.read_csv("galprop5.dat", sep=' ',comment='#', header = None
   )
45 g_prop5 = g_prop5.as_matrix()

47
#Stack the data together
49 data=np.concatenate((data1 ,data2 ,data3 ,data4 ,data5 ),axis=0)
   gal_prop=np.concatenate((g_prop1 ,g_prop2 ,g_prop3 ,g_prop4 ,g_prop5 ),axis
   =0)

51
#bins equally spaced in log space / written in lin space (stellar mass
   from 0.1 to 1.8 Msun)
53 m_bins=np.genfromtxt("bins.dat")
   #velocity dispersion bins with average 150,190,230,270,310 and +-20 km/s
55 sigma_bins=np.array([130,170,210,250,290,330])
   #Import Zstar from gal_prop
57 z_star=gal_prop[:,19]
   #####
59 #Use only early type galaxies <=> low sfr
   #####
61 #Requirement 1: Select galaxies with SFR/Mstar<10e-11 yr-1
   #Import the Mstar as lin
63 log_mstar=data[:,3]
   mstar=10**log_mstar
65 #Import sfr
   sfr=data[:,8]
67 #Find the indices of the galaxies
   gal_indi=np.where(np.divide(sfr ,mstar)<10e-11)
69
#Import the whole pdmf and select the pdmf for the galaxies that fit in
   requirement 1
71 pdmf=data[:,9:-1]
   pdmf=pdmf[gal_indi]
73 log_mstar=log_mstar[gal_indi]

```

```

z_star=z_star[ gal_indi ]
75 #Import the whole sigma and select the pdmf for the galaxies that fit in
    requirement 1
sigma=data[:,2]
77 sigma=sigma[ gal_indi ]
#Requirement 2: Find the galaxies that have sigma between 130 and 330
79 sigma_indi=np.where(np.logical_and(sigma>=130,sigma<=330))
#Final sigma and pdmf values for the galaxies that fit in requirement 1
    and 2
81 pdmf=pdmf[ sigma_indi ]
sigma=sigma[ sigma_indi ]
83 log_mstar=log_mstar[ sigma_indi ]
z_star=z_star[ sigma_indi ]
85 # Use galaxies with Mstar>9
mass_indi=np.where(log_mstar>=9)
87 pdmf=pdmf[ mass_indi ]
sigma=sigma[ mass_indi ]
89 log_mstar=log_mstar[ mass_indi ]
z_star=z_star[ mass_indi ]
91 #Calculate the median in each mass bin for every velocity dispersion bin
med=[]
93 #Std for each bin
std_med=[]
95 print(np.shape(pdmf),np.shape(sigma))

97 #Final Mstar and Z with values in different columns
M_star_final=[]
99 Z_star_final=[]

101 #Loop through the sigma bins
for i in range(len(sigma_bins)-1):
103     #Create an empty array for the median pdmf
    med_pdmf=[]
105     M_star_bin=[]
    Z_star_bin=[]
107     for j in range(len(sigma)):
        #Loop through all the galaxies and if sigma fits in the given
        bin, add the pdmf in the array
109         if(sigma[j]>=sigma_bins[i] and sigma[j]<=sigma_bins[i+1]):
            med_pdmf.append(pdmf[j,:])
            M_star_bin.append(log_mstar[j])
            Z_star_bin.append(z_star[j])
113
        #calculate the median pdmf as well as the standard deviation
115     med_imf=np.median(med_pdmf,axis=0)
    std=np.std(med_pdmf,axis=0)
117     # add it to the final array
    med.append(med_imf)
119     std_med.append(std)
    M_star_final.append(M_star_bin)
121     Z_star_final.append(Z_star_bin)

```



```

123 #Get from bins to points in the mass range (the average of 2 values in
    log space is the geometric average in lin space)
    m_points=[]
125 for i in range(len(m_bins)-1):
        m_points.append(np.sqrt(m_bins[i]*m_bins[i+1]))
127 m_points=np.log10(m_points)
    #Average mass in each mass bin
129 m_mean=[]
    for i in range(len(m_bins)-1):
131         m_mean.append(np.mean((m_bins[i]+m_bins[i+1])/2))

133 #Divide the median pdmf's for every sigma

135

137 #Function which calculates the error in every dN/dLogM point from the dM
    values
    def gamma_error(median, sigma_median):
139         err=np.multiply(0.434,np.divide(sigma_median,median))
        return err
141 #Separate the pmdfs and the errors for each sigma bin
    med_150=np.log10(np.divide(med[0],m_mean))
143 std_150=gamma_error(med[0],std_med[0])

145 med_190=np.log10(np.divide(med[1],m_mean))
    std_190=gamma_error(med[1],std_med[1])
147
149 med_230=np.log10(np.divide(med[2],m_mean))
    std_230=gamma_error(med[2],std_med[2])

151 med_270=np.log10(np.divide(med[3],m_mean))
    std_270=gamma_error(med[3],std_med[3])
153
155 med_310=np.log10(np.divide(med[4],m_mean))
    std_310=gamma_error(med[4],std_med[4])

157

159
    #Plotting the IMF for every sigma
161 plt.figure(figsize=(12,12))
    #Plot without errorbars
163 plt.plot(m_points,med_150,'ro',color='red',label=r"$\sigma=150$ $km/s$
        $and$ $\alpha=2.24$")
    plt.plot(m_points,med_190,'ro',color='black',label=r"$\sigma=190$ $km/s$
        $and$ $\alpha=2.40$")
165 plt.plot(m_points,med_230,'ro',color='blue',label=r"$\sigma=230$ $km/s$
        $and$ $\alpha=2.48$")
    plt.plot(m_points,med_270,'ro',color='green',label=r"$\sigma=270$ $km/s$
        $and$ $\alpha=2.53$")
167 plt.plot(m_points,med_310,'ro',color='orange',label=r"$\sigma=310$ $km/
        s$ $and$ $\alpha=2.53$")

```

```

#Plot with errorbars
169 #plt.errorbar(m_points, med_150, yerr=std_150, fmt='o', color='red', label=r"
    $\sigma=150\pm 20$ $km/s$")
    #plt.errorbar(m_points, med_190, yerr=std_190, fmt='o', color='red', label=r"
    $\sigma=190\pm 20$ $km/s$")
171 #plt.errorbar(m_points, med_230, yerr=std_230, fmt='o', color='red', label=r"
    $\sigma=230\pm 20$ $km/s$")
    #plt.errorbar(m_points, med_270, yerr=std_270, fmt='o', color='red', label=r"
    $\sigma=270\pm 20$ $km/s$")
173 #plt.errorbar(m_points, med_310, yerr=std_310, fmt='o', color='red', label=r"
    $\sigma=310\pm 20$ $km/s$")

#Legend and labels
175 plt.xlabel(r'$Log$ $M_{*}$', fontsize=23)
177 plt.ylabel(r'$\frac{dN}{dlogM}$', fontsize=26)
    plt.xlim(np.log10(0.1), np.log10(0.4))
179 plt.ylim(-0.5, 1)

#Fitting lines to IMF for every sigma value. Only for values between 0.1
    and 0.4 solar masses. The 18th element
    #corresponds to the 0.7M limit, the 12th element corresponds to 0.4
    solar masses.
183 def limit_slope(low_limit, high_limit):
    m_point_new=m_points[low_limit:high_limit]

185
    imf_150=med_150[low_limit:high_limit]
187 std_150_new=std_150[low_limit:high_limit]

    imf_190=med_190[low_limit:high_limit]
189 std_190_new=std_190[low_limit:high_limit]

    imf_230=med_230[low_limit:high_limit]
191 std_230_new=std_230[low_limit:high_limit]

    imf_270=med_270[low_limit:high_limit]
193 std_270_new=std_270[low_limit:high_limit]

    imf_310=med_310[low_limit:high_limit]
195 std_310_new=std_310[low_limit:high_limit]
    return m_point_new, imf_150, imf_190, imf_230, imf_270, imf_310,
    std_150_new, std_190_new, std_230_new, std_270_new, std_310_new
201

#I know this is a very weird way of doing it
203 m_points_1, imf_150_1, imf_190_1, imf_230_1, imf_270_1, imf_310_1, std_150_1,
    std_190_1, std_230_1, std_270_1, std_310_1=limit_slope(0, 18)
    m_points_2, imf_150_2, imf_190_2, imf_230_2, imf_270_2, imf_310_2, std_150_2,
    std_190_2, std_230_2, std_270_2, std_310_2=limit_slope(0, 12)
205 m_points_3, imf_150_3, imf_190_3, imf_230_3, imf_270_3, imf_310_3, std_150_3,
    std_190_3, std_230_3, std_270_3, std_310_3=limit_slope(11, 18)

207
#Line fitting where a*x+b=0

```

```

209 def lin_func(x,a,b):
    return a*x+b
211 #Initial guess. 0,0 for simplicity
x0=np.array([0.0, 0.0])
213
#Function which calculates the slope and intercept values as well as the
errors in them, using a weighted least square
215 def param_values(xdata,ydata,ystd):
    param=opt.curve_fit(lin_func,xdata,ydata,x0,ystd)
217     values=param[0]
    a=values[0]
219     b=values[1]
    pcov=param[1]
221     perr = np.sqrt(np.diag(pcov))
    aerr=perr[0]
223     berr=perr[1]
    return a,b,aerr
225 #Calculate the slope a, the intercept b and the error in the slope std
    for each bin
    #0.1-0.7
227 a1_1,b1_1,std1_1=param_values(m_points_1,imf_150_1,std_150_1)
    a2_1,b2_1,std2_1=param_values(m_points_1,imf_190_1,std_190_1)
229 a3_1,b3_1,std3_1=param_values(m_points_1,imf_230_1,std_230_1)
    a4_1,b4_1,std4_1=param_values(m_points_1,imf_270_1,std_270_1)
231 a5_1,b5_1,std5_1=param_values(m_points_1,imf_310_1,std_310_1)
    #0.1-0.4
233 a1_2,b1_2,std1_2=param_values(m_points_2,imf_150_2,std_150_2)
    a2_2,b2_2,std2_2=param_values(m_points_2,imf_190_2,std_190_2)
235 a3_2,b3_2,std3_2=param_values(m_points_2,imf_230_2,std_230_2)
    a4_2,b4_2,std4_2=param_values(m_points_2,imf_270_2,std_270_2)
237 a5_2,b5_2,std5_2=param_values(m_points_2,imf_310_2,std_310_2)
    #0.4-0.7
239 a1_3,b1_3,std1_3=param_values(m_points_3,imf_150_3,std_150_3)
    a2_3,b2_3,std2_3=param_values(m_points_3,imf_190_3,std_190_3)
241 a3_3,b3_3,std3_3=param_values(m_points_3,imf_230_3,std_230_3)
    a4_3,b4_3,std4_3=param_values(m_points_3,imf_270_3,std_270_3)
243 a5_3,b5_3,std5_3=param_values(m_points_3,imf_310_3,std_310_3)
245
#Print the IMF slope with the standard deviation
247 #print("IMF slope for sigma: 150=", -a1+1,"190=", -a2+1,"230=", -a3
    +1,"270=", -a4+1,"310=", -a5+1)
    #print("STD=",std1,std2,std3,std4,std5)
249 #Get the lines for the fit
    m1=np.multiply(m_points_2,a1_2)+b1_2
251 m2=np.multiply(m_points_2,a2_2)+b2_2
    m3=np.multiply(m_points_2,a3_2)+b3_2
253 m4=np.multiply(m_points_2,a4_2)+b4_2
    m5=np.multiply(m_points_2,a5_2)+b5_2
255 #Plot the lines over the data points
    plt.plot(m_points_2,m1,color='red',linewidth=1)
257 plt.plot(m_points_2,m2,color='black',linewidth=1)

```



```

plt.plot(m_points_2, m3, color='blue', linewidth=1)
259 plt.plot(m_points_2, m4, color='green', linewidth=1)
plt.plot(m_points_2, m5, color='orange', linewidth=1)
261 plt.grid()
print(a5_1, a5_2, a5_3)
263 ## -1.32968491193 -1.2411670839 -1.39176263458
## -1.4942263311 -1.40904255851 -1.55111688385
265 ## -1.5779696297 -1.48712424856 -1.63870761322
## -1.63172185674 -1.53289937492 -1.69785262867
267 ## -1.63215511227 -1.52639856457 -1.69759069844
plt.legend(fontsize=20, loc=3)
269

#####
#Compare with Spiniello et al. 2014
273 #####
#The Spiniello data
275 spin_imf=np.array([1.85, 2.08, 2.33, 2.40, 2.62])
spin_imf_err=np.array([0.2, 0.2, 0.4, 0.3, 0.4])
277 plt.figure(figsize=(17,7))
#This work data
279 imf_slope_1=np.array([-a1_1, -a2_1, -a3_1, -a4_1, -a5_1])+1
imf_slope_2=np.array([-a1_2, -a2_2, -a3_2, -a4_2, -a5_2])+1
281 imf_slope_3=np.array([-a1_3, -a2_3, -a3_3, -a4_3, -a5_3])+1
print(imf_slope_1, imf_slope_2, imf_slope_3)
283 #Plotting the errorbars
plt.errorbar([150, 190, 230, 270, 310], spin_imf, xerr=20, yerr=spin_imf_err,
            fmt='o', color='red', label='Spiniello et al. 2014')
285 plt.errorbar([150, 190, 230, 270, 310], imf_slope_1, xerr=20, yerr=np.multiply
            (5, [std1_1, std2_1, std3_1, std4_1, std5_1]), fmt='o', color='blue', label=
            '0.1-0.7')
plt.errorbar([150, 190, 230, 270, 310], imf_slope_2, xerr=20, yerr=np.multiply
            (5, [std1_2, std2_2, std3_2, std4_2, std5_2]), fmt='o', color='green', label
            ='0.1-0.4')
287 plt.errorbar([150, 190, 230, 270, 310], imf_slope_3, xerr=20, yerr=np.multiply
            (5, [std1_3, std2_3, std3_3, std4_3, std5_3]), fmt='o', color='black', label
            ='0.4-0.7')
#Function that fits Spiniello data, not used
289 def fun(x):
    return 2.3*np.log10(x/200)+2.1
a, b, c, d, e=ss.linregress(np.log10([150, 190, 230, 270, 310]), imf_slope_1)
291 sigmas=np.linspace(100, 330, 100)
#plt.plot(sigmas, np.multiply(np.log10(sigmas), a)+b)
#print("Slope =", a, "Intercept point =", b)
293 #Fits to the data points
#plt.plot(sigmas, fun(sigmas), color='red')
297 #plt.plot(sigmas, np.multiply(np.log10(sigmas), a)+b, color='blue')
### Plotting legend
299 plt.title(r"IMF slope as a function of $\sigma$", fontsize=20)
plt.xlabel(r"$\sigma$ (km/s)", fontsize=26)
301 plt.ylabel(r"$IMF$ slope $(\alpha)$", fontsize=26)
plt.grid()

```

```

303 plt.legend(loc=4, fontsize=20)
    #Plotting Sapleter and Chabrier
305 plt.plot([100,350],[2.35,2.35], '—', linewidth=2, color='black', label='
    Salpeter')
    plt.text(102, 2.37, 'Salpeter', fontsize=20)
307 plt.plot([100,350],[1.8,1.8], '—', linewidth=2, color='black', label='
    Chabrier')
    plt.text(200, 1.82, 'Chabrier-like', fontsize=20)
309
    ##
    #####

311 # Analytic solution comparison
    ##
    #####

313 plt.figure(figsize=(17,7))
    plt.errorbar([150,190,230,270,310], spin_imf, xerr=20, yerr=spin_imf_err,
        fmt='o', color='red', label='Spiniello et al. 2014')
315 plt.errorbar([150,190,230,270,310],[2.48,2.52,2.53,2.56,2.54], xerr=20,
        fmt='o', color='blue', label='Analytic Solution')
    plt.title(r"IMF slope as a function of  $\sigma$ ", fontsize=20)
317 plt.xlabel(r" $\sigma$  (km/s)", fontsize=26)
    plt.ylabel(r"$IMF$ slope  $(\alpha)$ ", fontsize=26)
319 plt.grid()
    plt.legend(loc=4, fontsize=20)
321 #Plotting Sapleter and Chabrier
    plt.plot([100,350],[2.35,2.35], '—', linewidth=2, color='black', label='
    Salpeter')
323 plt.text(102, 2.37, 'Salpeter', fontsize=20)
    plt.plot([100,350],[1.8,1.8], '—', linewidth=2, color='black', label='
    Chabrier')
325 plt.text(200, 1.82, 'Chabrier-like', fontsize=20)

327 #####
    # Analytic vs Numerical
329 #####

    plt.figure(figsize=(17,7))
331 plt.errorbar([150,190,230,270,310],[2.48,2.52,2.53,2.56,2.54], xerr=20,
        fmt='o', color='red', label='Analytic')
    plt.errorbar([150,190,230,270,310], imf_slope_1, xerr=20, yerr=np.multiply
        (5,[std1_1, std2_1, std3_1, std4_1, std5_1]), fmt='o', color='blue', label=
        'Numeric')
333 plt.title(r"IMF slope as a function of  $\sigma$ ", fontsize=20)
    plt.xlabel(r" $\sigma$  (km/s)", fontsize=26)
335 plt.ylabel(r"$IMF$ slope  $(\alpha)$ ", fontsize=26)
    plt.grid()
337 plt.legend(loc=4, fontsize=20)
    plt.plot([100,350],[2.35,2.35], '—', linewidth=2, color='black', label='
    Salpeter')
339 plt.text(102, 2.37, 'Salpeter', fontsize=20)

```

```

plt.plot([100,350],[1.8,1.8], '—', linewidth=2, color='black', label='
Chabrier')
341 plt.text(200, 1.82, 'Chabrier-like', fontsize=20)
plt.ylim(1.6,3.2)
343
#####
345 # Mass and metallicity histograms
#####
347 plt.figure(figsize=(10,10))
#bins=[9,9.5,10,10.5,11,11.5,12]
349 #Weights for the histograms
w_1=np.ones_like(M_star_final[0])/float(len(M_star_final[0]))
351 w_2=np.ones_like(M_star_final[1])/float(len(M_star_final[1]))
w_3=np.ones_like(M_star_final[2])/float(len(M_star_final[2]))
353 w_4=np.ones_like(M_star_final[3])/float(len(M_star_final[3]))
w_5=np.ones_like(M_star_final[4])/float(len(M_star_final[4]))
355 #####
bins=[9,9.5,10,10.5,11,11.5,12]
357 plt.hist(M_star_final[0], bins=bins, weights=w_1, fill=False, linewidth
=2,hatch='//', histtype='step',color='red',label='150')
plt.hist(M_star_final[1], bins=bins, weights=w_2, fill=False, linewidth
=2,hatch='\\\\', histtype='step',color='black',label='190')
359 plt.hist(M_star_final[2], bins=bins, weights=w_3, fill=False, linewidth
=1,hatch='—', histtype='step',color='blue',label='230')
plt.hist(M_star_final[3], bins=bins, weights=w_4, fill=False, linewidth
=1,hatch='\\\\', histtype='step',color='green',label='270')
361 plt.hist(M_star_final[4], bins=bins, weights=w_5, fill=False, linewidth
=4,hatch='//', histtype='step',color='orange',label='310')
plt.legend(loc=2,fontsize=15)
363 plt.xlabel(r'$Log\,M_{*}$', fontsize=23)
365
367
#For the metallicity, I had to remove the nan values from the array.
This is how I did it:
369 Z_star_150 = np.array(Z_star_final[0])
Z_star_150 = Z_star_150[~np.isnan(Z_star_150)]
371 Z_star_150 = np.log10(Z_star_150)
373
Z_star_190 = np.array(Z_star_final[1])
Z_star_190 = Z_star_190[~np.isnan(Z_star_190)]
375 Z_star_190 = np.log10(Z_star_190)
377
Z_star_230 = np.array(Z_star_final[2])
Z_star_230 = Z_star_230[~np.isnan(Z_star_230)]
379 Z_star_230 = np.log10(Z_star_230)
381
Z_star_270 = np.array(Z_star_final[3])
Z_star_270 = Z_star_270[~np.isnan(Z_star_270)]
383 Z_star_270 = np.log10(Z_star_270)

```

```

385 Z_star_310 = np.array(Z_star_final[4])
Z_star_310 = Z_star_310[~np.isnan(Z_star_310)]
387 Z_star_310 = np.log10(Z_star_310)
#Final array
389 Z_star_final=[Z_star_150,Z_star_190,Z_star_230,Z_star_270,Z_star_310]
#Weights for the histogram
391 W_1=np.ones_like(Z_star_final[0])/float(len(Z_star_final[0]))
W_2=np.ones_like(Z_star_final[1])/float(len(Z_star_final[1]))
393 W_3=np.ones_like(Z_star_final[2])/float(len(Z_star_final[2]))
W_4=np.ones_like(Z_star_final[3])/float(len(Z_star_final[3]))
395 W_5=np.ones_like(Z_star_final[4])/float(len(Z_star_final[4]))
#Plotting the figure
397 plt.figure(figsize=(10,10))
zbins=np.linspace(-0.1,0.3,10)
399 plt.hist(Z_star_final[0], bins=zbins, weights=W_1, fill=False, linewidth
        =2, hatch='//', histtype='step', color='red', label='150')
plt.hist(Z_star_final[1], bins=zbins, weights=W_2, fill=False, linewidth
        =2, hatch='\\\\', histtype='step', color='black', label='190')
401 plt.hist(Z_star_final[2], bins=zbins, weights=W_3, fill=False, linewidth
        =1, hatch='—', histtype='step', color='blue', label='230')
plt.hist(Z_star_final[3], bins=zbins, weights=W_4, fill=False, linewidth
        =1, hatch='\\\\', histtype='step', color='green', label='270')
403 plt.hist(Z_star_final[4], bins=zbins, weights=W_5, fill=False, linewidth
        =4, hatch='//', histtype='step', color='orange', label='310')
plt.legend(loc=2, fontsize=15)
405 plt.xlim(-0.1,0.3)
print(np.sum(a))
407 plt.xlabel(r'$Log\,Z_{*}$', fontsize=23)

409 #####
#Random galaxies with avg IMF
411 #####
#I've selected 15 random galaxies (using a random generator) and put
    them in a file
413 rand_150=np.genfromtxt("150_rand")
rand_190=np.genfromtxt("190_rand")
415 rand_230=np.genfromtxt("230_rand")
rand_270=np.genfromtxt("270_rand")
417 rand_310=np.genfromtxt("310_rand")
#Add the fit
419 fit_1=np.multiply(m_points_1,a1_1)+b1_1
fit_2=np.multiply(m_points_1,a2_1)+b2_1
421 fit_3=np.multiply(m_points_1,a3_1)+b3_1
fit_4=np.multiply(m_points_1,a4_1)+b4_1
423 fit_5=np.multiply(m_points_1,a5_1)+b5_1
#Plotting everything
425 width=0.5
plt.figure(figsize=(15,15))
427 #150
plt.subplot(3,2,1)
429 plt.title(r"$\sigma=150\,km/s$", fontsize=15)
for i in range(15):

```



```

431     plt.plot(m_points, rand_150[i], color='red', linewidth=width)
plt.errorbar(m_points, med_150, yerr=std_150, fmt='o', color='blue', label=r"
    Median IMF")
433 plt.xlim(np.log10(0.1), np.log10(0.7))
plt.ylim(-0.5, 1)
435 plt.legend(fontsize=15)
plt.grid()
437
#190
439 plt.subplot(3, 2, 2)
plt.title(r"$\sigma=190$, km/s", fontsize=15)
441 for i in range(15):
    plt.plot(m_points, rand_190[i], color='red', linewidth=width)
443 plt.errorbar(m_points, med_190, yerr=std_190, fmt='o', color='blue', label=r"
    Median IMF")
plt.xlim(np.log10(0.1), np.log10(0.7))
445 plt.ylim(-0.5, 1)
plt.legend(fontsize=15)
447 plt.grid()
#230
449 plt.subplot(3, 2, 3)
plt.title(r"$\sigma=230$, km/s", fontsize=15)
451 for i in range(15):
    plt.plot(m_points, rand_230[i], color='red', linewidth=width)
453 plt.errorbar(m_points, med_230, yerr=std_230, fmt='o', color='blue', label=r"
    Median IMF")
plt.xlim(np.log10(0.1), np.log10(0.7))
455 plt.ylim(-0.5, 1)
plt.legend(fontsize=15)
457 plt.grid()
#270
459 plt.subplot(3, 2, 4)
plt.title(r"$\sigma=270$, km/s", fontsize=15)
461 for i in range(15):
    plt.plot(m_points, rand_270[i], color='red', linewidth=width)
463 plt.errorbar(m_points, med_270, yerr=std_270, fmt='o', color='blue', label=r"
    Median IMF")
plt.xlim(np.log10(0.1), np.log10(0.7))
465 plt.ylim(-0.5, 1)
plt.legend(fontsize=15)
467 plt.grid()
#310
469 plt.subplot(3, 2, 5)
plt.title(r"$\sigma=310$, km/s", fontsize=15)
471 for i in range(15):
    plt.plot(m_points, rand_310[i], color='red', linewidth=width)
473 plt.errorbar(m_points, med_310, yerr=std_310, fmt='o', color='blue', label=r"
    Median IMF")
plt.xlim(np.log10(0.1), np.log10(0.7))
475 plt.ylim(-0.5, 1)
plt.legend(fontsize=15)
477 plt.grid()

```

```

#####
# THE END #
#####

```

6.2 The PDMF mass bins

Bin edges	M_{\odot}
1	0.1
2	0.11175828065
3	0.124899132938
4	0.139585123518
5	0.155997934086
6	0.174340608984
7	0.194840067075
8	0.21774990898
9	0.243353554392
10	0.271967748289
11	0.303946479409
12	0.339685359484
13	0.379626517378
14	0.424264068712
15	0.474150228607
16	0.529902143188
17	0.592209524353
18	0.661843182262
19	0.739664561093
20	0.826636396053
21	0.923834623454
22	1.03246169122
23	1.15386143447
24	1.28953570025
25	1.44116292696
26	1.61061890854
27	1.8

Table 6.1: The PDMF mass bins given in linear but equally spaced in logarithmic space.

7. References

- Auger, M.W. et al. *ApJ*, 721:L163, 2010.
- Bastian N., Covey K.R., Meyer M.R., *Annu. Rev. Astron. Astrophys.* 2010. 48:339-89.
- Benson, A.J., Galaxy formation theory, California Institute of Technology, 38-39, 2010.
- Benson, A.J., Lacey, C.G., Baugh, C.M., Cole, S., Frenk, C.S., 2002b. Monthly Notices of the Royal Astronomical Society 333, 156176.
- Benson, A.J., Nusser, A., Sugiyama, N., Lacey, C.G., 2001a. MNRAS 320, 153176.
- Benson, A.J., Pearce, F.R., Frenk, C.S., Baugh, C.M., Jenkins, A., 2001b. Monthly Notices of the Royal Astronomical Society 320, 261280.
- Bonnatto C., Bica E. 2007. *MNRAS* 337:1301
- Bouvier J, Stauffer JR, Martin EL, Barrado y Navascues D, Wallace B, Bejar VJS. 1998. *Astron. Astrophys.* 336:490
- Brandner W, Clark JS, Stolte A, Waters R, Negueruela I, Goodwin SP. 2008. *Astron. Astrophys.* 478:137
- Buchner, J., 4 November 2015
- Carrari G, Baume G, Piotto G, Mendez RA, Schmidtbreick L. 2005. *Astron. Astrophys.* 436:527
- Chabrier, H. *PASP*, 115:763, 2003
- Conroy, C. and van Dokkum, P. *ApJ*, 747:69, 2012a.
- Conroy, C. and van Dokkum, P. *ApJ*, 760:71, 2012b.
- D. Maoz, F. Mannucci, 2012. MNRAS
- Devriendt, J.E.G., Sethi, S.K., Guiderdoni, B., Nath, B.B., 1998. MNRAS 298, 708718.
- Espinoza P, Selman FJ, Melnick J. 2009. *Astron. Astrophys.* 501:563
- Faber, S. M.; Jackson, R. E., Velocity dispersions and mass-to-light ratios for elliptical galaxies, *Astrophysical Journal*, vol. 204, Mar. 15, 1976, pt. 1, p. 668-683.
- Faber, S.M. and French, H.B., Possible M dwarf enrichment in the semistellar nucleus of M31. *Astrophys.J.* 235,405-412, 1980.

- Ferreras, I. et al. *MNRAS*, 429:L15, 2013.
- Figer DF, Kim SS, Morris M, Serabyn E, Rich RM, McLean IS. 1999. *Ap. J.* 525:750
- Ghez AM, Duchene G, Matthews K, Hornstein SD, Tanner A, et al. 2003. *Ap. J. L.* 586:L127
- Gliese w, Jahreiss H. 1991. On *The Astronomical Data Center CD-ROM: Selected Astronomical Catalogs*, Vol. I, ed. LE Brotzmann.
- Helly, J.C., Cole, S., Frenk, C.S., Baugh, C.M., Benson, A., Lacey, C., Pearce, F.R., 2003b. *MNRAS* 338, 913925.
- Hubble, E.P. (1936). *The realm of the nebulae*, Yale University Press
- Kalirai JS, Fahlman GG, Richer HB, Ventura P. 2003. *Astron. J.* 126:1402
- Kauffmann, G., Guiderdoni, B., White, S.D.M., 1994. *MNRAS* 267, 981 Devriendt, J.E.G., Guiderdoni, B., 2000. *A&A* 363, 851862.
- Klypin A. A., Trujillo-Gomez S., Primack J., 2011, *ApJ*, 740, 102
- Kroupa P, Tout CA, Gilmore G. 1993. *MNRAS* 262:545
- Krumholz M.R., 2011. *arXiv*:1109.1564
- LaBarbera, F. et al. *MNRAS*, 433:3017, 2013.
- Loeckmann U, Baumgardt H, Kroupa P. 2010. *MNRAS* 402:519
- Maciejewski G., Niedzielski A. 2007. *Astron. Astrophys.* 467:1065
- Morau E, Bouvier J, Stauffer JR, Cuillandre J-C. 2003. *Astron. Astrophys.* 400:891
- Morris M. 1993. *Ap. J.* 408:496
- NASA, ESA, and The Hubble Heritage Team (STScI/AURA); J. Blakeslee (Washington State University)
- Offner, S. S. R. et al., *The origin and universality of the stellar initial mass function*, University of Arizona Press, 2014
- Pandey AK, Upadhyay K, Ogura K, Sagar R, Mohan V, et al. 2005. *MNRAS* 358:1290
- Phelps RL, Janes KA. 1993. *Astron. J.* 106:1870
- Popping G., Rachel S. Somerville, Maud Galametz, 2016, *arXiv*:1609.08622
- Popping G., Somerville R. S., Trager S. C., 2014, *MNRAS*, 442, 2398
- Porter L. A., Somerville R. S., Primack J. R., Johansson P. H., 2014, *MNRAS*, 444, 942
- Prisinzano L, Micela G, Sciortino S, Favata F. 2003. *Astron. Astrophys.* 404:927
- Reid IN, Gizis JE. 1997. *Astron. J.* 124:2721
- Salpeter, Edwin E., *The Luminosity Function and Stellar Evolution*, *Astrophysical Journal*, vol. 121, p.161, 01/1955
- Sanner J, Geffert M, Brunsendorf J, Schmoll J. 1999. *Astron. Astrophys.* 349:448
- Sanner J, Geffert M. 2001. *Astron. Astrophys.* 370:87
- Santo JFC Jr, Bonatto C, Bica E. 2005. *Astron. Astrophys.* 349:448
- Scalo J. 2005. See Corbelli, Pala and Zinnecker 2005, p.23.
- Schiavon, R.P., barbuy, B., Rossi, S.C.F. and Milone, A., *The near-infrared Na I doublet feature in M stars. Astrophys.J.* 479,902-908, 1997.
- Schiavon, R.P. Barbuy, B. and Singh, P.D., *The FeH Wing-Ford band in spectra of M stars. Astrophys.J.* 484, 499-510, 1997.
- Schodel R, Ott T, Genzel R, Eckart A, Mouawad N, Alexander T. 2003. *Ap. J.* 596:1015
- Somerville, R.S., 2002. *ApJ* 572, L23L26. Li, Y., Lucia, G.D., Helmi, A., 2010. *Monthly*

-
- Notices of the Royal Astronomical Society 401, 20362052.
- Somerville, R.S., Livio, M., 2003. *ApJ* 593, 611615
- Benson, A.J., Sugiyama, N., Nusser, A., Lacey, C.G., 2006. *MNRAS* 369, 10551080.
- Somerville R. S., Gilmore R. C., Primack J. R., Dominguez A., 2012, *MNRAS*, 423, 1992
- Somerville R. S., Hopkins P. F., Cox T. J., Robertson B. E., Hernquist L., 2008b, *MNRAS*, 391, 481
- Somerville R. S., Popping G., Trager S. C., 2015, *MNRAS*, 453, 4337
- Somerville R. S., Primack J. R., 1999, *MNRAS*, 310, 1087
- Somerville R. S., Primack J. R., Faber S. M., 2001, *MNRAS*, 320, 504
- Spiniello, C., Trager, S. C., Koomans, L. V. E., and Conroy, C. *MNRAS*, 438:1438, 2014.
- Spiniello, C. et al. *ApJL*, 753:L32, 2012.
- Stolte A, Grebel EK, Brandner W, Figer DF. 2002. *Astron. Astrophys.* 394:459
- Stringer, M.J., Brooks, A.M., Benson, A.J., Governato, F., 2010. arXiv 1001.0594S.
- Treu, T. et al. *ApJ*, 709:1195, 2010.
- Trujillo-Gomez S., Klypin A., Primack J., Romanowsky A. J., 2011, *ApJ*, 742, 16
- van de Kamp P. 1971 *Annu. Rev. Astron. Astrophys.* 9:103
- van Dokkum, P. and Conroy, C. *Nature*, 468:940, 2010.
- White, S. D. M., & Rees, M. J. 1978, *MNRAS*, 183, 341
- Wingm R.F. and Ford, W.K., The infrared spectrum of the cool dwarf Wolf 359. *Publ. Astron.Soc.Pacif.* 81, 527-529, 1969.
- Yoshida, N., Stoehr, F., Springel, V., White, S.D.M., 2002. Monthly Notices of the Royal Astronomical Society 335, 762772.